PAPER

Sulfation effect of Ce/TiO₂ catalyst for the selective catalytic reduction of NOₓ with NH₃: mechanism and kinetic studies†

Wenjie Zhang, [ID] [a] Guofu Liu,[a] Jie Jiang,[b] Yuchen Tan,[c] Qi Wang,[d] Chenghong Gong,[e] Dekui Shen [ID] *[a] and Chunfei Wu*[f]

Ceria-based catalysts are competitive substitutes for the commercial SCR catalysts due to their high SCR activity and excellent redox performance. For a better understanding of the SO₂ poisoning mechanism over ceria-based catalysts, the sulfation effect of the Ce/TiO₂ catalyst on the SCR activity over a wide reaction temperature range was systematically studied *via* comprehensive characterizations, *in situ* DRIFT studies and kinetic studies. The results demonstrated that the NO conversion at 150 °C is significantly inhibited by the formation of cerium sulfites/sulfates due to the inhibited redox properties and excessive adsorption of NH₃, which restrict the dissociation of NH₃ to NH₂, resulting in a much lower reaction rate of E−R reaction over the sulfated Ce/TiO₂ catalyst. With the increase in the reaction temperature, the reaction rate of the E−R reaction significantly increased due to the improved redox properties and weakened adsorption of NH₃. Moreover, the rate of the C−O reaction over the sulfated Ce/TiO₂ catalysts is obviously lower than that of the fresh Ce/TiO₂ catalyst. The promotion of NO conversion over the sulfated catalyst at 330 °C is attributed to both the increase in the reaction rate of E−R reaction and the inhibition of the C−O reaction.

1. Introduction

Selective catalytic reduction (SCR) by ammonia has been proven to be the most efficient technology for removing NOₓ that originates from stationary and mobile pollution sources.[1] SCR catalysts are the core of the NH₃-SCR system, and the commercial SCR catalyst based on the VO₅–WO₃/TiO₂ catalyst has been widely used for the NH₃-SCR system. However, the high operating temperature (>350 °C), the toxicity of vanadium and the low N₂ selectivity at high temperatures restrict the use of vanadium-based catalysts on industry boiler systems, which is urgently needed for the removal of NOₓ in China.[2] Therefore, significant efforts have been made to develop environmentally

benign catalysts with a superior low-temperature SCR activity, such as Fe₂O₃-based,[3] CeO₂-based,[4] CuO-based[5] and MnOₓ-based catalysts.[6]

Ceria-based catalysts have been considered as potential candidates for the replacement of V₂O₅–WO₃/TiO₂ due to their high oxygen storage capacity and excellent redox properties. A series of ceria-based catalysts, including CeO₂/TiO₂, CeO₂–WO₃, Sb–V₂O₅–CeO₂/TiO₂ and CeO₂–SnOₓ, have shown superior middle-temperature SCR activity and N₂ selectivity.[7–9] However, the presence of a low concentration of SO₂ in the flue gas could cause an inevitable deactivation effect on NO conversion over ceria-based catalysts. The sulfation of ceria-based catalysts can slightly promote SCR performance by the enhancement of the acidity and the reactivity of cerium sulfates on the premise of sufficient redox properties.[10] In most cases, it has been found that ceria-based catalysts are sensitive to SO₂ poisoning and a good amount of cerium sulfites/sulfates are deposited on the surface of catalysts,[8,11] blocking the catalyst pore channels and cutting off the redox cycle involved in the standard SCR reaction. A previous investigation by Muhammad *et al.*[9] simply studied the sulfation effect of the Ce/TiO₂ catalyst and Ti/CeO₂ catalyst on SCR activity, suggesting that the low-temperature SCR activity is much more sensitive to the formation of cerium sulfites/sulfates, while middle and high-temperature SCR activities are less affected. It was demonstrated that the sulfation effects of the ceria-based catalyst on NO conversion at different reaction temperatures are different, while the insight

[a]Key Laboratory of Energy Thermal Conversion and Control of Ministry of Education, School of Energy and Environment, Southeast University, Nanjing 210096, Jiangsu, PR China. E-mail: 101011398@seu.edu.cn

[b]Engineering Laboratory of Energy System Process Conversion & Emission Control Technology of Jiangsu Province, School of Energy and Mechanical Engineering, Nanjing Normal University, Nanjing 210042, PR China

[c]Nanjing Foreign Language School, Nanjing 210018, Jiangsu, PR China

[d]College of Metrological Technology and Engineering, China Jiliang University, Hangzhou 310018, PR China

[e]Jiangsu Yanxin SCI-TECH Co., Ltd, WuXi 214426, PR China

[f]School of Chemistry and Chemical Engineering, Queen's University Belfast, Belfast BT7 1NN, UK. E-mail: c.wu@qub.ac.uk

into the sulfation effect on the SCR activity was not revealed. Moreover, the SCR reaction mechanism of the sulfated Ce/TiO$_2$ catalyst may differ from that of a fresh catalyst.

In order to investigate the sulfation effect of the Ce/TiO$_2$ catalyst on the SCR activity and the reaction mechanism over a wide reaction temperature range, the SCR activities of the fresh Ce/TiO$_2$ catalyst and sulfated catalyst were studied. The sulfation effect of the Ce/TiO$_2$ catalyst was fully investigated via N$_2$ physisorption, XPS, H$_2$-TPR, NH$_3$-TPD and in situ DRIFT. Furthermore, kinetic studies involving the E–R mechanism, L–H mechanism, nonselective catalytic reduction reaction (i.e., NSCR reaction) and catalytic oxidation reaction (i.e., the C–O reaction) were performed for a clearer understanding of the sulfation effect of the Ce/TiO$_2$ catalyst on the SCR reaction. It is expected that the present study will help in understanding the deactivation mechanism of sulfation at different reaction temperatures and further provide useful guidance for the design of catalysts with higher SO$_2$ resistance.

2. Experimental

2.1 Catalyst preparation

The Ce/TiO$_2$ catalyst (Ce/Ti mole ratio = 0.25) was prepared by a single step sol–gel method using butyl titanate (Sichuan Kelong, China), anhydrous ethanol acetic acid, deionized water, nitric acid and a certain amount of cerium nitrate. The chemicals were mixed under continuous and vigorous stirring at room temperature. After 3 h, a transparent yellowish sol was formed and was then aged for 12 h, which then became a gel. The derived sample was dried at 90 °C for 12 h to form a xerogel, followed by calcination at 450 °C at a heating rate of 10 °C min^{-1} in air for 6 h. Finally, the catalyst was crushed and sieved to 40–80 mesh size. The sulfated Ce/TiO$_2$ catalyst was pretreated in a flow of 1000 ppm SO$_2$ and 3% O$_2$ (750 mL min^{-1}) at 180 °C and 240 °C for 8 h, respectively, followed by flushing with N$_2$ for 1 h to remove the physically adsorbed SO$_2$. These catalysts were assigned as 180 °C-sulfated and 240 °C-sulfated catalysts, respectively.

2.2 Catalyst characterizations

2.2.1 XRD analysis. Powder X-ray diffraction measurements of the catalysts were performed using a computerized PANalytical X'Pert Pro diffractometer with Cu Kα (λ = 0.15406 nm) radiation.

2.2.2 BET analysis. N$_2$ adsorption–desorption isotherms were obtained at −196 °C over the whole range of relative pressures using a JW-BK112 instrument (Beijing JWGB Sci. & Tech. Co. Ltd, China). Prior to N$_2$ adsorption, the catalysts were pre-treated at 150 °C for 5 h. Specific areas were computed from adsorption/desorption isotherms using the BET equation. Pore volumes and average pore diameters were computed by applying the BJH method from the adsorption branches of the isotherms.

2.2.3 XPS analysis. The content and chemical states of surface compositions were determined by X-ray photoelectron spectroscopy (XPS) using an ESCALAB Mark II spectrometer (Vacuum Generators,

UK) with Al KR radiation (1486.6 eV). The binding energy was corrected using contaminated carbon (BE = 284.6 eV).

2.2.4 H$_2$-TPR analysis. Hydrogen-temperature programmed reduction (H$_2$-TPR) was performed using a FineSorb 3010D chemisorption analyzer (FINETEC instruments, China). First, the catalyst (60 mg) was pre-treated at 300 °C in a flow of Ar (20 mL min^{-1}) for 1 h and cooled to 50 °C. Then, the temperature was raised linearly to 800 °C at the rate of 10 °C min^{-1} in a flow of 10 vol% H$_2$/Ar (20 mL min^{-1}). The H$_2$ consumption was monitored by TCD.

2.2.5 XRF analysis. The S content of the sulfated Ce/TiO$_2$ catalyst was determined by the XRF method using an Energy-Dispersive XRF spectrometer (Thermo Scientific, ARL QUANT'X with an Rh anode, X-rays of 4–50 kV (1 kV step), 1 mm size beam). A 3.5 mm Si(Li) drifted crystal with Peltier cooling (−88 °C was used as a detector).

2.2.6 NH$_3$-TPD analysis. Temperature programmed desorption of ammonia (NH$_3$-TPD) was performed using a FineSorb 3010D chemisorption analyzer (FINETEC instruments, China). First, the sample (80 mg) was pre-treated in He (20 mL min^{-1}) at 300 °C for 1 h. After cooling to 80 °C, the sample was exposed to a flow of 5 vol% NH$_3$/N$_2$ (20 mL min^{-1}) for 30 min, followed by He purging for another 1 h. Finally, the temperature was raised to 650 °C in He flow at the rate of 10 °C min^{-1}. The amount of ammonia desorbed from the catalysts was monitored using a thermal conductivity detector (TCD).

2.2.7 In situ DRIFTS analysis. The in situ DRIFT experiments were performed on a NicoletNexus 5700 FTIR spectrometer using a diffuse reflectance attachment (HARRICK) equipped with a reaction cell (ZnSe windows). Each spectrum was collected by averaging 8 scans with a 4 cm^{-1} resolution to ensure high temporal resolution while maintaining a reasonable signal to noise ratio. Each sample was pre-treated under a N$_2$ atmosphere at 400 °C for 1 h and then cooled down to 240 °C or 150 °C. Subsequently, (1) for the adsorption/desorption of NH$_3$, 600 ppm of NH$_3$ was injected into the IR cell for 40 min at 150 °C until saturation, followed by a N$_2$ purge for 10 min and then heating to 200, 250, 300, 350 and 400 °C. The spectra were recorded based on the Kubelka–Munk function, with reference to the background spectra recorded in N$_2$ at the corresponding temperatures. (2) For the reaction of NH$_3$ + O$_2$ with pre-adsorbed NO, after the pretreatment at 400 °C, 600 ppm NO was injected into the IR cell for 40 min until saturation, followed by N$_2$ purging for 10 min and then NH$_3$ + O$_2$ were added; the spectra were also recorded. This procedure is similar to the reaction of NO + O$_2$ with pre-adsorbed NH$_3$.

2.3 SCR activity estimation of catalyst samples

The NH$_3$-SCR reaction and studies of the effect of SO$_2$ on the SCR reaction were performed in a fixed-bed quartz tube reactor. The reactor consists of a quartz tube with an inner diameter of 16 mm and a thermocouple placed on the outside wall of the reactor to control the temperature of the furnace. About 1 mL of catalyst (40–80 mesh) was used in all experiments. The reaction conditions were as follows: 1 mL of catalyst, 600 ppm NO, 600 ppm NH$_3$, 3 vol% O$_2$, N$_2$ as the balance, 1000 ppm SO$_2$ (if

required) and a gas hourly space velocity (GHSV) of 40 000 h^{-1}. NO$_x$, NH$_3$ and N$_2$O in the effluent gas were analyzed using a flue gas analyzer (Testo 350), Nessler's reagent spectrophotometry method[12] and a N$_2$O analyzer (Medi-Gas G200) when the reaction system reached a steady state for 30 min. The NO$_x$ conversion (η), N$_2$O selectivity (S) and the pseudo-first-order rate constant (τ) were calculated using the following formulae:

$$\eta = \left(1 - \frac{[NO + NO_2]_{out}}{[NO + NO_2]_{in}}\right) \times 100\% \quad (1)$$

$$S = \frac{2[N_2O]_{out}}{[NH_3]_{in} - [NH_3]_{out} + [NO_x]_{in} - [NO_x]_{out}} \times 100\% \quad (2)$$

$$\tau = -\frac{V}{W} \times \ln(1 - \eta) \quad (3)$$

where V was the total flow rate (mL s^{-1}), and W was the mass of the catalyst used in the experiment (g).

2.4 Experiments for kinetic studies

To obtain the kinetic parameters of the SCR reaction, the NSCR reaction and catalytic oxidation reaction (*i.e.*, the C–O reaction), and steady-state kinetic studies were performed. The inlets consisted of 0–600 ppm NO, 600 ppm NH$_3$ and 3% O$_2$ with N$_2$ as the balance. A very high GHSV of 600–2400 dm^3 g^{-1} h^{-1} (the total flow rate was 750 mL min^{-1} and the loading of the catalysts were 33–135 mg) was used to exclude the diffusion limitation (including the internal and external diffusion). The steady-state kinetic experiments were performed in the temperature range of 150–400 °C. The concentrations of outlet NH$_3$ and N$_2$O were obtained *via* the Nessler's reagent spectrophotometry method[12] and N$_2$O analyzer (Medi-Gas G200).

3. Results and discussion

3.1 Catalytic performance

Fig. 1 illustrates the NO conversion, NH$_3$ conversion and N$_2$O selectivity of fresh and sulfated Ce/TiO$_2$ catalysts. For the fresh Ce/TiO$_2$ catalyst (Fig. 1A), it shows excellent SCR activity, which

is higher than 75% in the temperature range of 180–330 °C. The higher NH$_3$ conversion as compared to NO conversion at each temperature suggests that a part of the NH$_3$ was oxidized to NO and N$_2$O due to the catalytic oxidation (*i.e.*, C–O reaction) and NSCR reaction, contributing to the decrease in the NO conversion with the increase in the reaction temperature to 330 °C. As for the sulfated Ce/TiO$_2$ catalyst (Fig. 1B), a much more severely inhibited low-temperature SCR activity was observed. The reduced NO conversions for the sulfated catalyst with respect to fresh Ce/TiO$_2$ were 75.6%, 66.2%, 45.5%, 36.8% and 26.8% at 150 °C, 180 °C, 210 °C, 240 °C, 270 °C, respectively, indicating that the sulfation effect of the Ce/TiO$_2$ catalyst on NO conversion is greatly dependent on the reaction temperature. The lower the reaction temperature, the greater the negative effects of sulfation. Moreover, it was noted that the sulfated catalyst showed higher NO conversion, as compared to the fresh catalyst, at 330 °C, which was also reported in a previous study;[13] the fresh Ce/TiO$_2$ showed a decrease in NO conversion with the increase in reaction temperature from 300 to 330 °C. The sulfated Ce/TiO$_2$ catalyst showed a lower N$_2$O selectivity (lower than 13%) in the temperature range of 150–330 °C as compared with the fresh Ce/TiO$_2$ catalyst. This result demonstrates that the sulfation of the Ce/TiO$_2$ catalyst significantly inhibits the low-temperature SCR activity while showing a higher SCR activity at 330 °C as compared to the fresh Ce/TiO$_2$ catalyst by inhibiting the catalytic oxidation of NH$_3$ to NO. The SCR performance and N$_2$O selectivity of the 240 °C-sulfated catalyst are similar to those of the 180 °C-sulfated catalyst shown in Fig. S1.†

3.2 Characterisations of the catalysts before and after SO$_2$ sulfation

3.2.1 XRD and BET analysis. XRD patterns of the fresh and sulfated Ce/TiO$_2$ catalysts are shown in Fig. S2.† All the catalysts exhibited characteristic TiO$_2$-anatase [PDF-ICDD 21-1272]. The peaks corresponding to CeO$_2$ could not be detected, indicating that the ceria is well dispersed on the catalysts. The intensity of the TiO$_2$ diffraction peaks of sulfated catalysts is stronger than that of fresh Ce/TiO$_2$ catalyst, indicating the higher crystallinity
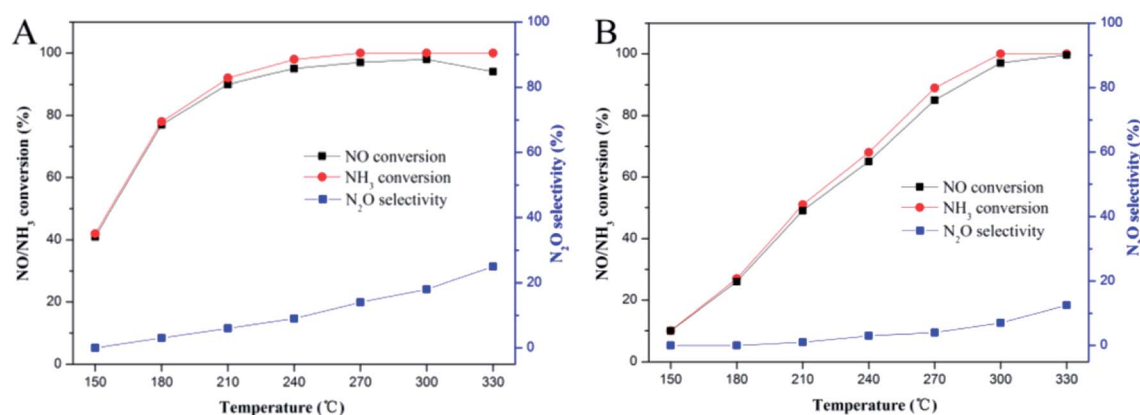

Fig. 1 SCR performance and N$_2$O selectivity of (A) fresh Ce/TiO$_2$ and (B) 180 °C-sulfated Ce/TiO$_2$. Reaction conditions: [NH$_3$] = [NO] = 600 ppm, [O$_2$] = 3%, N$_2$ balance, GHSV = 40 000 h^{-1}.

Fig. 2   XPS results for (A) Ce3d, (B) Ti2p, (C) S2p, and (D) O1s of the fresh and sulfated catalysts.

include an intense peak located at 529.5 eV and a faint peak at 531.1 eV over the fresh Ce/TiO$_2$ catalyst, which represent lattice oxygen (O^{2-}, denoted as O$_\beta$) and chemisorbed oxygen or weakly bonded oxygen species (O$_2{}^{2-}$ or O$^-$, denoted as O$_\alpha$), respectively. After sulfation treatment, the binding energies of O$_\alpha$ and O$_\beta$ shift towards higher values (0.3–0.7 eV), which is due to the stronger affinity of S bonded to the oxygen species. As shown in Table 2, the surface concentration of lattice oxygen follows an upward trend from 26.7% to 43.6% and 42.9%, respectively, as along with the Ce^{3+}/Ce ratio. Generally, O$_\alpha$ is generated during the transition from Ce^{4+} to Ce^{3+} according to the following

reaction: 2Ce^{4+} + 2O^{2-} ↔ 2Ce^{4+} + O$_2$ + 2e$^-$/V$_d{}^{2+}$ ↔ Ce^{3+}–V$_d$–Ce^{3+} + O$_2$. The symbol V$_d$ represents the defects and oxygen vacancies generated from the removal of lattice oxygen due to the formation of Ce$_2$(SO$_4$)$_3$.

3.2.3 H$_2$-TPR. The redox properties of the catalyst are key factors determining the low-temperature activity of SCR.[24] In order to find out the effects of cerium sulfates/sulfites on the redox properties of Ce/TiO$_2$ catalyst, H$_2$-TPR experiments were conducted and the reduction profiles are shown in Fig. 3. The fresh Ce/TiO$_2$ catalyst exhibited one overlapped reduction peak centered at 465 °C (starting from 250 °C and ending at 688 °C),

Table 2   The surface compositions of the samples derived from XPS data

Sample (Ce/TiO$_2$)	Atomic concentration (at%)				Atomic ratio (%)		
	Ce	Ti	O	S	Ce^{3+}/Ce	O$_\alpha$/(O$_\alpha$ + O$_\beta$)	Bulk S^a
Fresh	6.07	24.95	68.97	—	25.6	26.7	0
180 °C-sulfated	4.92	19.92	69.14	6.01	30.9	43.6	1.4
240 °C-sulfated	5.07	20.20	70.31	4.42	26.9	42.9	1.7

^{a} Atomic ratio of S on the bulk of samples from XRF characterization.

which is very similar to other reports.[25,26] The overlapped reduction peak can be ascribed to the stepwise reduction of surface oxygen species. At 250 °C, the reduction of lattice oxygen of stoichiometric ceria (Ce^{4+}–O–Ce^{4+}) begins. With the increase in the reduction temperature, the reduction of ceria (Ce^{3+}–O–Ce^{4+}) to ceria (Ce^{3+}–O–Ce^{3+}) begins with the elimination of lattice oxygen.[27] For the 180 °C-sulfated Ce/TiO$_2$ catalyst, the reducibility was severely inhibited as compared to the fresh Ce/TiO$_2$ catalyst; the reduction peak at 465 °C disappeared and an intense reduction peak located at 645 °C was observed, which can be attributed to the reduction of surface cerium sulfates/sulfites. This suggests that the lattice oxygen may react with the sulfur to form cerium sulfates/sulfites since no reduction peak assigned to lattice oxygen was observed.[28] After the sulfation treatment at 240 °C, the reduction peak at 465 °C still existed but the peak strength decreased with the narrowed reduction temperature range between 410 °C and 520 °C. More SO$_2$ reacted with the deeper interior of ceria to form bulk-like and bulk cerium sulfites/sulfates with the increase in sulfation temperature to 240 °C,[18] which is in line with the XPS results shown in Table 2.

3.2.4 Surface acidity. Another crucial factor of low-temperature SCR activity is the surface acidity of the catalyst. NH$_3$-TPD and NH$_3$-DRIFT have been used to characterize the amount and the strength of the acid sites of the catalysts. The NH$_3$-TPD profile is shown in Fig. 4, where two NH$_3$ desorption peaks at 215 °C and 590 °C can be observed with the increase in temperature over the fresh Ce/TiO$_2$ catalyst. The strength of the acidity is indicated by the desorption temperature. The region below 200 °C is assigned to the weak acidities and above 300 °C can be assigned to the strong acidities. Accordingly, the fresh Ce/TiO$_2$ catalyst has mainly medium-strength acidities. After sulfation treatment, three desorption peaks were found; the first was centered at 242 °C and the intensity was further strengthened as compared to the fresh Ce/TiO$_2$ catalyst. The second peak was centered at 587 °C and an additional NH$_3$ desorption peak centered at 420 °C was observed. Moreover,

compared to the 240 °C-sulfated catalyst, the 180 °C-sulfated catalyst had more adsorbed NH$_3$. This can be attributed to the presence of more cerium sulfates/sulfites on the surface of the catalyst.

It is believed that the capacity for NH$_3$ adsorption is related to the surface area of the catalyst. The enhanced capacity of NH$_3$ adsorption and the higher desorption temperature indicate the changes in the acid sites for NH$_3$ adsorption after sulfation treatment. In order to further investigate the changes in acid sites over the fresh catalyst and the sulfated catalysts, *in situ* DRIFTS was performed during the NH$_3$ adsorption/desorption within the temperature range from 150 °C to 400 °C, shown in Fig. S4.† The main characteristic vibrations of NH$_3$ adsorption over the fresh Ce/TiO$_2$ catalyst are at 1680 cm^{-1}, 1598 cm^{-1}, and 1170 cm^{-1} (Fig. S4(A)†). The band at 1680 cm^{-1} can be attributed to the symmetric stretching vibration of NH$_4^+$ species on Bronsted acid sites,[29,30] while the band at 1598 cm^{-1} can be assigned to the formation of nitrate intermediates due to the excessive catalytic oxidation of NH$_3$ by lattice oxygen.[31] The band at 1170 cm^{-1} can be assigned to the symmetric stretching vibration of NH$_3$ adsorbed on the Lewis acid sites. The bands at 3100–3400 cm^{-1} are attributed to the vibrations of N–H bonds, and the negative bands due to the O–H vibrations at 3716 and 3658 cm^{-1} also showed up. For the sulfated catalysts shown in Fig. S4(B),† several bands at 1000–1700 cm^{-1} and 3100–3700 cm^{-1} were seen. The band at 1670 cm^{-1} and 1432 cm^{-1} could be due to the symmetric and asymmetric stretching vibrations of N–H bonds adsorbed on the Bronsted acid sites.[32,33] These vibrations are related to the adsorbed SO$_2$ on the unsaturated metallic sites, which further provide more sites for the adsorption of H and further form S–OH groups to form the Bronsted acid sites.[34] The bands at 1319 cm^{-1}, 1262 cm^{-1} and 1096 cm^{-1} could be assigned to the vibrations of NH$_3$ adsorbed on Lewis acid sites. Two negative bands centered at 3708 cm^{-1} and 3666 cm^{-1} can be assigned to the consumption of Ce–OH due to NH$_3$ adsorption. The other negative band at 1367–1351 cm^{-1} can be attributed to NH$_3$ adsorption on O=S=O on
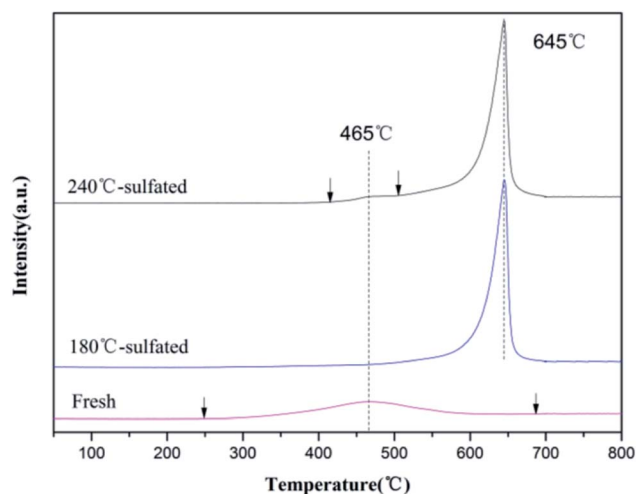

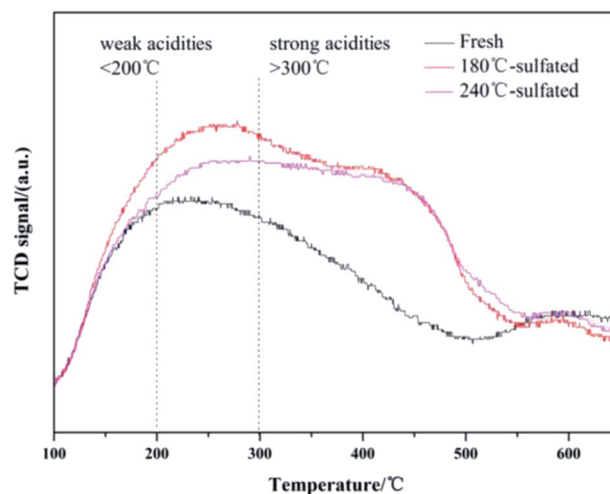**Fig. 3** H$_2$-TPR profiles of the fresh and sulfated catalysts.

Fig. 4 NH$_3$-TPD profiles of fresh and sulfated catalysts.

the surface of SO_4^{2-} sites.[35] With the increase in the temperature of the IR cell (from 150 to 400 °C), the intensity of the negative band at 1367–1351 cm^{-1} gradually decreased due to the desorption of NH_3 from surface SO_4^{2-} sites. It should be noted that after the sulfation treatment, the band at 1598 cm^{-1} still exists on the catalyst but the strength of the peak is significantly reduced, indicating that the excessive catalytic oxidation of NH_3 was inhibited after the sulfation treatment.

The integration of the peaks at 1300–1150 cm^{-1} (for Lewis acid sites), 1432 cm^{-1} (for Bronsted acid sites over sulfated catalysts) and 1680 cm^{-1} (for Bronsted acid sites over fresh Ce/TiO$_2$ catalyst) were calculated. As shown in Table S1,† there are significantly more Bronsted acid sites on the sulfated catalysts as compared to the fresh Ce/TiO$_2$, which are 5.54 *vs.* 0.62, respectively. The negative band of O=S=O provides more Bronsted acid sites in the sacrifice of Lewis acid sites. Thus, the Lewis acid sites of the sulfated catalysts almost disappear, which are 0.48 *vs.* 4.47 with respect to the fresh catalyst, respectively. Moreover, it can be speculated that for the fresh Ce/TiO$_2$ catalyst, the peak centered at 214 °C as shown in Fig. 4 could be attributed to the desorption of NH_3 on the Lewis acid sites and the peak at 598 °C could be assigned to the desorption of NH_4^+ on the Bronsted acid sites. After sulfation, the peak at 242 °C can be assigned to NH_3 desorbed from Lewis acid sites and most NH_4^+ desorbed from Bronsted acid sites. Therefore, it is suggested that the peak centered at 430 °C could be assigned to NH_3 desorbed from strong Bronsted acid sites.

3.3 Reaction mechanism study by *in situ* DRIFTS

3.3.1 Reaction between $NH_3 + O_2$ and the adsorbed NO species. Transient reactions were carried out to investigate the reactivity of the adsorbed reactants in the SCR reaction. The evolution of DRIFTS spectra for the reaction between $NH_3 + O_2$ and adsorbed NO are shown in Fig. 5. After purging with NO for 40 min, the fresh Ce/TiO$_2$ catalyst was mainly covered by adsorbed NO$_2$ (at 1617 cm^{-1}), bidentate nitrate (at 1558 cm^{-1}) and monodentate nitrito (O–N–O–, at 1232 cm^{-1}). The bands of NO$_2$ and nitrate/nitrito showed little change with the introduction of $NH_3 + O_2$. After purging with $NH_3 + O_2$ for 4 min, the band associated with the monodentate nitrito group disappeared and a new band at 1197 cm^{-1} was observed, which was assigned to the adsorption of NH_3 on Lewis acid sites. It is suggested that the reactivity of the adsorbed NO$_x$ species over the fresh Ce/TiO$_2$ catalyst is restricted, indicating that the L–H reaction pathway is inhibited over the fresh Ce/TiO$_2$ catalyst.

As for the 180 °C-sulfated catalyst, several bands at 1612, 1434, 1365 and 1288 cm^{-1} were observed as shown in Fig. 5B. These can be assigned to surface nitrate species (1612 cm^{-1} for NO$_2$, 1365 cm^{-1} for free NO$_3^-$ (ref. 36)). The negative band at 1434 cm^{-1} and 1288 cm^{-1} can be assigned to NO adsorption on the S=O of surface SO_4^{2-} sites. With the introduction of $NH_3 + O_2$, the intensity of the negative bands gradually decreased due to the desorption of NO from surface SO_4^{2-} sites, indicating that the adsorbed NO on SO_4^{2-} is reactive. It can be seen that the intensities of NO$_2$ and nitrates obviously decreased with the introduction of $NH_3 + O_2$. Moreover, the adsorbed NH_3/NH_4^+

and nitrite/nitrate species on the surface of the sulfated catalyst cannot coexist. This could be due to the reaction between adsorbed nitrite/nitrate species with NH_3 to form NH_4NO_3 and then decompose to N$_2$ and H$_2$O,[37] suggesting that the reaction between adsorbed NO and gaseous NH_3 can proceed by the L–H reaction pathway. Moreover, the negative band at 1361 cm^{-1} can be attributed to NH_3 adsorption on the S=O of the surface SO_4^{2-} sites. It is speculated that the NO adsorption on O=S=O causes the vibrations of S=O and O–N, contributing to the shift in the vibration of SO_4^{2-} from 1434 cm^{-1} to 1361 cm^{-1}. The integration area of the adsorbed NO bands have been calculated and are shown in Fig. S5.† It can be seen that the reactivity of adsorbed NO over the fresh Ce/TiO$_2$ catalyst was inhibited and the nitrite/nitrate formed on the sulfated Ce/TiO$_2$ catalyst was reactive during the SCR reaction.

3.3.2 Reaction between $NO + O_2$ and the pre-adsorbed NH_3 species. The evolution of the DRIFTS spectra for the reaction between $NO + O_2$ and adsorbed NH_3 is shown in Fig. 6. For the fresh Ce/TiO$_2$ catalyst, NH_3 is mainly adsorbed on the Lewis acid sites to form coordinated NH_3 (at 1180 cm^{-1}) after purging with 600 ppm NH_3 for 40 min. The band at 1598 cm^{-1} is attributed to the formation of nitrate intermediates due to the excessive catalytic oxidation of NH_3 by lattice oxygen as mentioned above. With the introduction of $NO + O_2$, both the NH_3 adsorbed on the Lewis acid sites and NH_4^+ on Bronsted sites gradually decrease. After 60 min, the Ce/TiO$_2$ catalyst is mainly covered by adsorbed NO$_2$ (at 1619 cm^{-1}), bidentate nitrate (at 1554 cm^{-1}), monodentate nitrate (at 1369 cm^{-1}) and monodentate nitrito groups (at 1232 cm^{-1}). It is suggested that the reaction between adsorbed NH_3 and gaseous NO over fresh Ce/TiO$_2$ catalyst follows the E–R reaction pathway. As for the 180 °C-sulfated catalyst, NH_3 is mainly adsorbed on the Bronsted acid sites to form NH_4^+ (at 1434 cm^{-1} and 1697 cm^{-1}) after purging with 600 ppm NH_3 for 40 min. The negative band at 1358 cm^{-1} can be assigned to NH_3 adsorption on S=O of the surface of SO_4^{2-} sites.[35] With the introduction of $NO + O_2$, the intensity of the negative band at 1358 cm^{-1} decreased gradually, indicating that the adsorbed NH_3 on SO_4^{2-} is reactive. After 60 min, all of the peaks associated with NH_3 bands disappeared and new bands at 1613 cm^{-1}, 1430 cm^{-1} and 1361 cm^{-1} were observed. The negative band at 1430 cm^{-1} can be assigned to NO adsorption on S=O of the surface SO_4^{2-} sites.

The integration areas of the adsorbed NH_3 bands were calculated and are shown in Fig. 7. It can be seen from Fig. 7A that the intensities of the coordinated NH_3 and NH_4^+ decreased rapidly. For the sulfated Ce/TiO$_2$ catalyst, the bands associated with NH_3 and NH_4^+ decreased slowly and still existed after purging with $NO + O_2$ for 30 min, suggesting that the E–R reaction pathway between the adsorbed NH_3 and gaseous NO was inhibited in spite of the enhanced acidity over the 180 °C-sulfated catalyst.

3.4 Kinetic studies

During the SCR reaction, the nonselective catalytic reduction reaction (NSCR reaction) and the catalytic oxidation of NH_3 to NO (*i.e.*, C–O reaction) may happen simultaneously. Therefore,
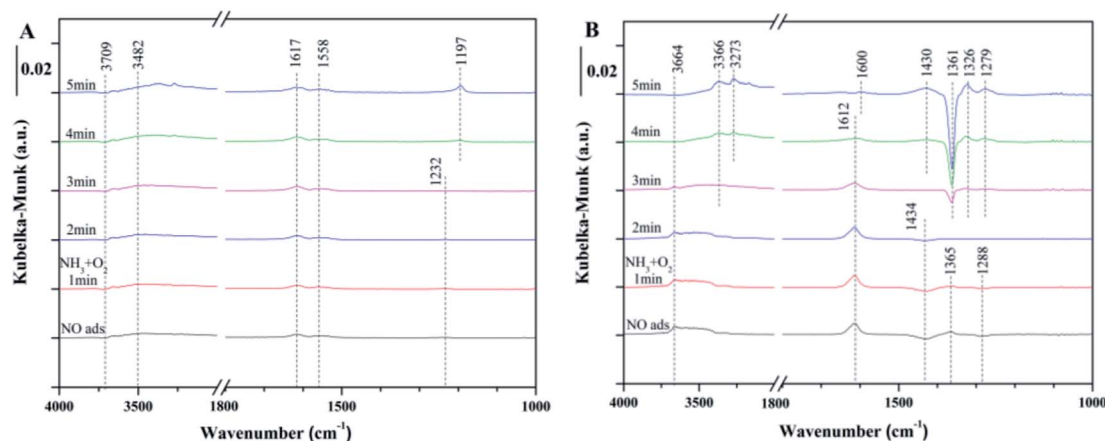
Fig. 5 *In situ* DRIFTS of the reaction between $NH_3 + O_2$ and pre-adsorbed NO at 240 °C over (A) fresh Ce/TiO_2, and (B) 180 °C-sulfated catalysts.

in order to further identify the contribution of the SCR reaction following the L–H reaction pathway and the E–R reaction pathway, NSCR reaction and the C–O reaction over the fresh and sulfated Ce/TiO_2 catalyst, the steady-state kinetic studies were performed as shown in Fig. S6 and S7.† It can be seen that the NH_3 conversion rate (δ_{NH_3}), NO_x conversion rate (δ_{NO}) and N_2O formation rate (δ_{N_2O}) over the fresh and the sulfated catalysts increased with the increase in NO concentration. The rate of the SCR reaction (δ_{SCR}) also increased and exhibited a linear relationship with the NO concentration (the correlation coefficients are higher than 0.99), indicating that the reaction order of the SCR reaction in relation to the gaseous NO concentration is 1. Moreover, the rate of the C–O reaction (δ_{C-O}) decreased with the increase in gaseous NO concentration, indicating that the reaction order of the C–O reaction in relation to the gaseous NO concentration is less than zero.

The SCR reaction, C–O reaction and NSCR reaction all contribute to NH_3 conversion. Thus, the NH_3 conversion rate can be described as

$$\delta_{NH_3} = \delta_{SCR} + \delta_{C-O} + \delta_{NSCR} \tag{4}$$

Both the SCR reaction and NSCR reaction contribute to the NO_x conversion, while the C–O reaction contributes to the formation of NO_x. Thus, the NO conversion rate can be described as

$$\delta_{NO} = \delta_{SCR} + \delta_{NSCR} - \delta_{C-O} \tag{5}$$

Therefore, the rates of SCR and C–O reaction can be described as

$$\delta_{SCR} = \frac{\delta_{NH_3} + \delta_{NO}}{2} - \delta_{NSCR} \tag{6}$$

$$\delta_{C-O} = \frac{\delta_{NH_3} - \delta_{NO}}{2} \tag{7}$$

The kinetic models of the L–H reaction, E–R reaction, NSCR reaction and C–O reaction over the fresh Ce/TiO_2 catalyst and the sulfated Ce/TiO_2 catalyst are shown in ESI.† All the reaction paths have been widely recognized and are suitable for the ceria-based catalyst.[38] According to eqn (10S) and (11S),† the
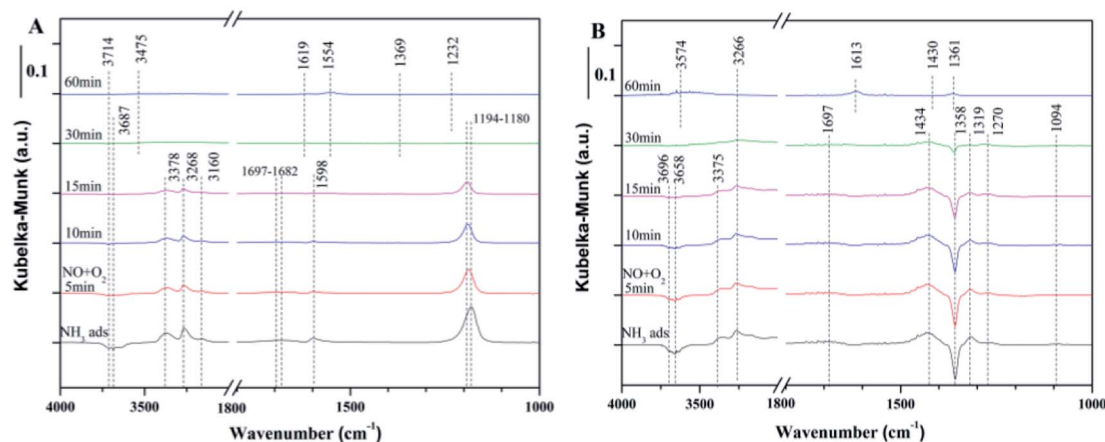

Fig. 6 *In situ* DRIFTS of the reaction between $NO + O_2$ and the pre-adsorbed NH_3 at 240 °C over (A) fresh Ce/TiO_2, (B) 180 °C sulfated catalyst.
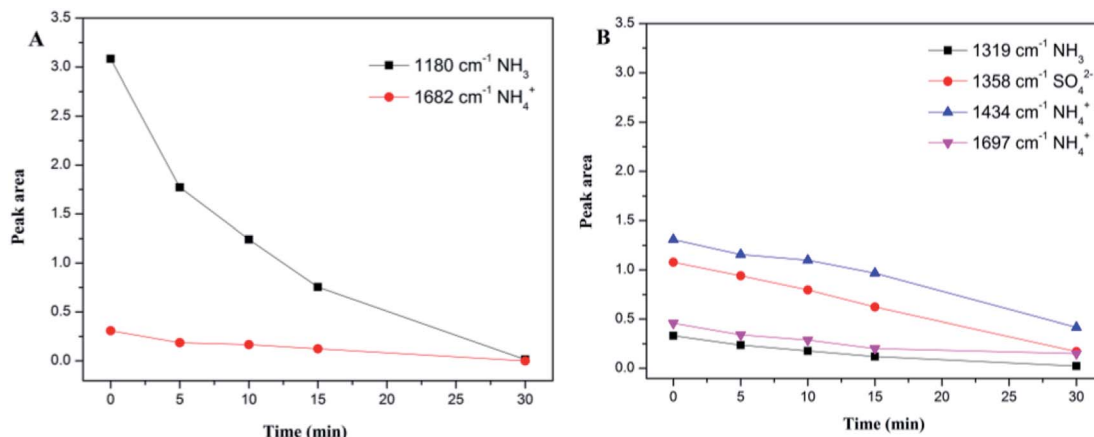
Fig. 7 Integration area from *in situ* DRIFTS of the reaction between NO + O$_2$ and pre-adsorbed NH$_3$ over (A) fresh Ce/TiO$_2$, (B) 180 °C sulfated catalyst.

rate of the SCR reaction over the ceria-based catalyst can be described as

$$\delta_{SCR} = \frac{d[N_2]}{dt}\bigg|_{E-R} + \frac{d[N_2]}{dt}\bigg|_{L-H}$$

$$= k_3[NO_{(g)}][NH_2] + k_{10}[Ce^{3+} - O - NO - NH_3]$$

$$= k_{E-R}[NO_{(g)}] + k_{L-H} \qquad (8)$$

The rate of the NSCR reaction over the ceria-based catalyst can be described as

$$\delta_{NSCR} = \frac{d[N_2O]}{dt} = \frac{k_4 k_5[NH_2]}{k_5[NO] + k_6}[NO_{(g)}][Ce^{4+}=O]$$

$$= \frac{k_4[NH_2][Ce^{4+}=O]}{1 + \frac{k_6}{k_5[NO_{(g)}]}} \qquad (9)$$

The rate of C–O reaction over the Ce/TiO$_2$ catalyst can be described as

$$\delta_{C-O} = \frac{d[NO]}{dt} = \frac{k_6 k_4[NH_2]}{k_5[NO_{(g)}] + k_6}[Ce^{4+}=O]$$

$$= \frac{k_4[NH_2][Ce^{4+}=O]}{\frac{k_5[NO_{(g)}]}{k_6} + 1} \qquad (10)$$

It can be seen from Fig. S6(D) and S7(D)† that the rate of the SCR reaction calculated according to eqn (6) is linear with the gaseous NO concentration (the correlation coefficients are higher than 0.99), which is in line with eqn (8). The parameters of k_{L-H} and k_{E-R} of the SCR reaction were calculated by the linear fitting of Fig. S6(D) and S7(D),† and the results are shown in Table 3.

According to eqn (8), k_{L-H} is dependent on k_{10} and the concentration of surface NH$_4$NO$_2$. k_{10} increases rapidly with the increase in the reaction temperature and thus, k_{L-H} increased

with the increase in reaction temperature as shown in Table 3. The *in situ* DRIFTS results in Fig. 6 demonstrate that the reactivity of NO adsorbed on the fresh Ce/TiO$_2$ catalyst at 240 °C is restricted, while the reaction between the adsorbed NO and gaseous NH$_3$ over the sulfated Ce/TiO$_2$ catalyst can proceed by the L–H reaction pathway due to the formation of NH$_4$NO$_2$ and its decomposition to N$_2$ and H$_2$O. Thus, the NH$_4$NO$_2$ formed on the sulfated Ce/TiO$_2$ catalysts was much more than that on the fresh Ce/TiO$_2$ catalyst at 240 °C, contributing to the higher concentration of the surface NH$_4$NO$_2$ over the sulfated Ce/TiO$_2$ catalyst. Therefore, the k_{L-H} value of the sulfated Ce/TiO$_2$ catalyst at 250 °C is higher than that of the fresh Ce/TiO$_2$ catalyst. With the increase in the reaction temperature, the chemical bonds between NO and the fresh Ce/TiO$_2$ catalyst may be activated, facilitating the formation of NH$_4$NO$_2$ over the fresh Ce/TiO$_2$ catalyst. Thus, the k_{L-H} value of the fresh Ce/TiO$_2$ catalyst is higher than that of the sulfated Ce/TiO$_2$ catalyst.

According to eqn (16S),† the k_{E-R} value is dependent on k_3 and the concentration of surface NH$_2$. According to eqn (12S),† the concentration of surface NH$_2$ is mainly related to the oxidation of surface Ce^{4+}, k_2 and the concentration of adsorbed NH$_3$. With the increase in the reaction temperature, the oxidation of Ce^{4+} and k_2 increased while the adsorption of NH$_3$ decreased. Thus, the concentration of surface NH$_2$ may show a peak value with the increase in reaction temperature, contributing to the peak value of k_{E-R} at 350 °C as shown in Table 3, which is in line with previous study.[39] For the sulfated Ce/TiO$_2$ catalyst, the promotion of acidity is more pronounced at middle temperatures than that at low temperatures as shown in Fig. 4. Thus, the concentration of surface NH$_2$ may increase further, contributing to the increased k_{E-R} with the increase in the reaction temperature to 400 °C.

3.5 The mechanism of the SCR performance of the fresh Ce/TiO$_2$ catalyst is better than that of sulfated Ce/TiO$_2$

Table 3 shows that the rate constant of the E–R reaction (k_{E-R}) is much higher than that of the L–H reaction (k_{L-H}), suggesting that the E–R reaction mechanism dominates in the standard

Table 3   Kinetic parameters of the SCR reaction over fresh Ce/TiO$_2$ and sulfated Ce/TiO$_2$

| | Temperature/°C | $\delta_{SCR} = k_{E-R}[NO_{(g)}] + k_{L-H}$ | | | |
		k_{L-H}	$k_{E-R}/10^6$	R^2	$\delta_{C-O}([NO] = 600\ ppm)$
Ce/TiO$_2$	150	3.61	0.008	0.995	1.31
	200	3.71	0.059	0.996	4.72
	250	4.672	0.165	0.998	19.90
	300	20.05	0.238	0.999	30.45
	350	89.16	0.443	0.999	62.69
	400	188.76	0.436	0.999	191.95
Sulfated Ce/TiO$_2$	150	0.151	0.003	0.997	0.19
	200	0.53	0.022	0.998	3.33
	250	14.84	0.043	0.999	15.49
	300	18.22	0.153	0.999	27.41
	350	87.53	0.414	0.999	50.6
	400	133.91	0.539	0.999	128.25

SCR reaction. According to kinetic studies, the contribution of the C–O reaction and the NSCR reaction at low temperature can be neglected. Therefore, the severely inhibited low-temperature NO conversion of the sulfated Ce/TiO$_2$ catalyst is due to the inhibited reaction rate of the SCR reaction, more precisely, the reaction rate of the E–R reaction. According to eqn (12S),† the concentration of NH$_2$ is dependent on k_2, the concentration of Ce^{4+}=O and the adsorbed NH$_3$. The H$_2$-TPR results suggest that the reducibility of the sulfated Ce/TiO$_2$ was severely inhibited, indicating that the rate constant of reaction (2S)† (k_2) over the sulfated Ce/TiO$_2$ catalyst is much lower than that over the fresh Ce/TiO$_2$ catalyst. The XPS results show that the concentration of the surface Ce^{4+}=O over the sulfated Ce/TiO$_2$ is less than that over the fresh Ce/TiO$_2$ catalyst. NH$_3$-TPD suggests that the concentration of NH$_3$ adsorbed on the sulfated Ce/TiO$_2$ catalyst is higher as compared to the fresh Ce/TiO$_2$ catalyst, which is approximately 1.18 times that of the fresh Ce/TiO$_2$ catalyst according to the NH$_3$-DRIFT results (Table S1†). Thus, the concentration of NH$_2$ over the sulfated Ce/TiO$_2$ catalyst is much lower than that over the fresh Ce/TiO$_2$ catalyst and, therefore, the k_3[NH$_2$] over sulfated Ce/TiO$_2$ is much lower than that over fresh Ce/TiO$_2$ catalyst, contributing to the much lower reaction rate of the E–R reaction (reaction (3S)†). It is suggested that reaction (2S)† is the rate-determining step in the SCR reaction following the E–R reaction pathway. In conclusion, the reason for the inhibited low-temperature performance with enhanced NH$_3$ adsorption is as follows. Firstly, the NH$_3$-TPD results demonstrate that the sulfated Ce/TiO$_2$ catalyst has significantly more strongly acidic sites as compared to the fresh Ce/TiO$_2$ catalyst. The strong binding of NH$_3$ to the sulfated Ce/TiO$_2$ catalyst restricts its reactivity with gaseous NO, which is hard to overcome for reaction (2S)† to proceed. Secondly, the formation of cerium sulfites/sulfates inhibited the reduction rate of Ce^{4+} to Ce^{3+} after the sulfation treatment, resulting in the inhibition of the reaction rate of reaction (2S)† (k_2).

With the increase in the reaction temperature to 350 °C, although the adsorbed NH$_3$ desorbed from the surface of the fresh and sulfated Ce/TiO$_2$ catalyst, the adsorption of NH$_3$ over the sulfated Ce/TiO$_2$ catalyst at middle temperatures was

obviously greater than that over the fresh Ce/TiO$_2$ catalyst. Moreover, the weaker binding of NH$_3$ with the sulfated Ce/TiO$_2$ catalyst promoted the reactivity of the adsorbed NH$_3$ with gaseous NO and the redox properties of the sulfated Ce/TiO$_2$ catalyst was significantly enhanced, suggesting that more adsorbed NH$_3$ dissociated into NH$_2$ according to reaction (2S).† Thus, the reaction rate of the E–R reaction pathway over the sulfated Ce/TiO$_2$ catalyst was close to that over the fresh Ce/TiO$_2$ catalyst. Moreover, the rate of the C–O reaction of the sulfated Ce/TiO$_2$ catalyst was obviously lower than that of the fresh Ce/TiO$_2$ catalyst, shown in Fig. S6(E) and S7(E).† Therefore, NO conversion at 330 °C over the sulfated catalyst was higher than that over the fresh Ce/TiO$_2$ catalyst. The promotion of NO conversion over the sulfated catalyst at 330 °C, as shown in Fig. 1, is attributed to both the increase in the reaction rate of the E–R reaction and the inhibition of the C–O reaction.

4.   Conclusions

The sulfation effect of the Ce/TiO$_2$ catalyst on NO conversion was found to be dependent on the reaction temperature. Significantly inhibited low-temperature SCR activity and enhanced SCR activity at higher temperature were found. Comprehensive characterizations, *in situ* DRIFT studies and kinetic studies were performed to investigate the mechanisms of these inhibiting and enhancing effects. It can be concluded that the different sulfation effects of the Ce/TiO$_2$ on SCR activity at different reaction temperatures can be attributed to the different reaction rates of the E–R reaction (k_{E-R}). At 150 °C, the contribution of the C–O reaction and the NSCR reaction can be neglected. The severely inhibited low-temperature SCR activity is due to the inhibited redox properties and excessive adsorption of NH$_3$, which restrict the dissociation of NH$_3$ to NH$_2$, contributing to the much lower reaction rate of the E–R reaction over the sulfated Ce/TiO$_2$ catalyst. With the increase in the reaction temperature, the reaction rate of the E–R reaction (k_{E-R}) significantly increased due to the improved redox properties and the weakened binding of NH$_3$ with the sulfated Ce/TiO$_2$ catalyst. Moreover, the C–O reaction rate of the sulfated Ce/TiO$_2$

catalyst is lower than that of the fresh Ce/TiO$_2$ catalyst. Therefore, NO conversion at 330 °C over the sulfated catalyst is higher than that over the fresh Ce/TiO$_2$ catalyst. It was demonstrated that the promotion of the NO conversion over the sulfated catalyst at 330 °C is attributed to both the increase in the reaction rate of the E–R reaction and the inhibition of the C–O reaction.

Conflicts of interest

There are no conflicts to declare.

Acknowledgements

References

1 W. Müller, H. Ölschlegel, A. Schäfer, N. Hakim and K. Binder, *Selective catalytic reduction-Europe's NO$_x$ reduction technology*, Report 0148-7191, SAE Technical Paper, 2003.

2 J. Li, H. Chang, L. Ma, J. Hao and R. T. Yang, *Catal. Today*, 2011, **175**, 147–156.

3 Y. Chen, C. Li, J. Chen and X. Tang, *Environ. Sci. Technol.*, 2018, **52**, 11796–11802.

4 X. Li, X. Li, J. Li and J. Hao, *Chem. Eng. J.*, 2017, **317**, 70–79.

5 B. Li, Z. Ren, Z. Ma, X. Huang, F. Liu, X. Zhang and H. Yang, *Catal. Sci. Technol.*, 2016, **6**, 1719–1725.

6 S. Deng, T. Meng, B. Xu, F. Gao, Y. Ding, L. Yu and Y. Fan, *ACS Catal.*, 2016, **6**, 5807–5815.

7 C. Li, G. Zeng, Y. Zhou and X. Zhang, *Appl. Surf. Sci.*, 2015, **342**, 174–182.

8 D. W. Kwon, K. B. Nam and S. C. Hong, *Appl. Catal., B*, 2015, **166**, 37–44.

9 M. S. Maqbool, A. K. Pullur and H. P. Ha, *Appl. Catal., B*, 2014, **152**, 28–37.

10 L. Zhang, L. Li, Y. Cao, X. Yao, C. Ge, F. Gao, Y. Deng, C. Tang and L. Dong, *Appl. Catal., B*, 2015, **165**, 589–598.

11 L. Xu, C. Wang, H. Chang, Q. Wu, T. Zhang and J. Li, *Environ. Sci. Technol.*, 2018, **52**, 7064–7071.

12 Shenyang Environmental Monitoring Central Station, *Industry standard-environmental protection*, 2009, HJ 533-2009.

13 F. Liu, K. Asakura, H. He, W. Shan, X. Shi and C. Zhang, *Appl. Catal., B*, 2011, **103**, 369–377.

14 K. S. Sing, *Pure Appl. Chem.*, 1985, **57**, 603–619.

15 M. Thommes, *Chem. Ing. Tech.*, 2010, **82**, 1059–1073.

16 A. Pfau and K. Schierbaum, *Surf. Sci.*, 1994, **321**, 71–80.

17 M. Y. Smirnov, A. V. Kalinkin, A. V. Pashis, A. M. Sorokin, A. S. Noskov, K. C. Kharas and V. I. Bukhtiyarov, *J. Phys. Chem. B*, 2005, **109**, 11712–11719.

18 L. Zhang, W. Zou, K. Ma, Y. Cao, Y. Xiong, S. Wu, C. Tang, F. Gao and L. Dong, *J. Phys. Chem. C*, 2014, **119**, 1155–1163.

19 E. García-Bordejé, J. L. Pinilla, M. J. Lázaro, R. Moliner and J. L. G. Fierro, *J. Catal.*, 2005, **233**, 166–175.

20 E. J. Romano and K. H. Schulz, *Appl. Surf. Sci.*, 2005, **246**, 262–270.

21 W. Wei, W. Ye, J. Wang, C. Huang, J.-B. Xiong, H. Qiao, S. Cui, W. Chen, L. Mi and P. Yan, *ACS Appl. Mater. Interfaces*, 2019, **11**(5), 4900–4907.

22 G. Zhang, W. Han, H. Zhao, L. Zong and Z. Tang, *Appl. Catal., B*, 2018, **226**, 117–126.

23 W. Wei, W. Chen, L. Ding, S. Cui and L. Mi, *Nano Res.*, 2017, **10**, 3726–3742.

24 H. Wang, X. Chen, S. Gao, Z. Wu, Y. Liu and X. Weng, *Catal. Sci. Technol.*, 2013, **3**, 715–722.

25 M. E. Yu, C. Li, G. Zeng, Y. Zhou, X. Zhang and Y. E. Xie, *Appl. Surf. Sci.*, 2015, **342**, 174–182.

26 P. Li, Y. Xin, Q. Li, Z. Wang, Z. Zhang and L. Zheng, *Environ. Sci. Technol.*, 2012, **46**, 9600–9605.

27 B. Murugan and A. V. Ramaswamy, *J. Phys. Chem. C*, 2008, **112**, 20429–20442.

28 J.-a. Wang, Z.-l. Zhu and C.-l. Li, *J. Mol. Catal. A: Chem.*, 1999, **139**, 31–41.

29 L. Dall Acqua, I. Nova, L. Lietti, G. Ramis, G. Busca and E. Giamello, *Phys. Chem. Chem. Phys.*, 2000, **2**, 4991–4998.

30 G. Ramis, L. Yi and G. Busca, *Catal. Today*, 1996, **28**, 373–380.

31 M. A. Larrubia, G. Ramis and G. Busca, *Appl. Catal., B*, 2000, **27**, L145–L151.

32 W. Hu, X. Gao, Y. Deng, R. Qu, C. Zheng, X. Zhu and K. Cen, *Chem. Eng. J.*, 2016, **293**, 118–128.

33 K. Hadjiivanov, *Catal. Rev.*, 2000, **42**, 71–144.

34 S. T. Choo, Y. G. Lee, I. S. Nam, S. W. Ham and J. B. Lee, *Appl. Catal., A*, 2000, **200**, 177–188.

35 N. Y. Topsoe, H. Topsoe and J. A. Dumesic, *J. Catal.*, 1995, **151**, 226–240.

36 M. P. Ruggeri, T. Selleri, M. Colombo, I. Nova and E. Tronconi, *J. Catal.*, 2015, **328**, 258–269.

37 I. Nova, C. Ciardelli, E. Tronconi, D. Chatterjee and B. Bandl-Konrad, *Catal. Today*, 2006, **114**, 3–12.

38 L. Ma, C. Y. Seo, M. Nahata, X. Chen, J. Li and J. W. Schwank, *Appl. Catal., B*, 2018, **232**, 246–259.

39 S. Xiong, X. Xiao, Y. Liao, H. Dang, W. Shan and S. Yang, *Ind. Eng. Chem. Res.*, 2015, **54**, 11011–11023.